大規模並列計算による乱流中の高分子モデルの挙動解析 (乱流研究 次の10年 : 乱流の動的構造の理解へ向けて)

AUTHOR(S):

WATANABE, Takeshi; GOTOH, Toshiyuki

数理解析研究所講究録
第1771巻 2011年 10-23

大規模並列計算による乱流中の高分子モデルの挙動解析

名古屋工業大学大学院創成シミュレーション工学専攻
渡邊 威 (Takeshi WATANABE) watanabe@nitech.ac.jp
後藤 俊幸 (Toshiyuki GOTOH) gotoh.toshiyuki@nitech.ac.jp
Department of Scientific and Engineering Simulation, Nagoya Institute of Technology

Abstract

The effects of polymer additives on decaying isotropic turbulence were numerically investigated using a hybrid approach. The approach consisted of a Brownian dynamics simulation with an enormous number of dumbbells and a turbulence DNS with large-scale parallel computations. A reduction of the energy dissipation rate and modification of the kinetic energy spectrum were observed when the reactions of the polymers were incorporated into the fluid motion. It was shown that the increase of concentration of polymers or of Weissenberg number yielded more modifications of turbulence statistics. We also observed that the generation of intense vortices was suppressed by polymer additives, being consistent with the previous studies using constitutive equations. It was found that the field structures of polymer stress field depended on the intensity of fluctuation, sheet-like structures for the intermediate intensity region or filamentary ones for intense region. We found the results with few polymers and large replicas could approximate those with many polymers and smaller replicas as far as the large-scale statistics were concerned.

1 Introduction

It is well known that small amounts of polymers added to a fluid significantly affect the large-scale flow structures, *i.e.*, turbulence drag reduction [1, 2, 3] or enhancing the mixing in the microchannel devices [4, 5, 6]. The later is due to the generation of random flows with low Reynolds numbers caused by elastic instability, so called the elastic turbulence [7, 8, 9]. On the other hand for larger Reynolds numbers, it is shown that the bulk of turbulence is affected by polymer additives, suggesting the modification of energy transfer dynamics over the inertial range scales [10].

It is vital to examine the meso-scale dynamics of polymers in turbulent flows for deep insight into the peculiar flow nature of dilute polymer solutions. The previous studies have been investigating the single polymer dynamics in a simple shear [11, 12, 13] and random flows [14, 15, 16, 17, 18, 19, 20]. The coil-stretch transition is an important concept to understand the polymer dynamics in turbulence [21]. In the case for simple shear flow, the polymer takes the coiled configuration if the shear intensity S is smaller than $1/\tau_s$ where τ_s is the characteristic relaxation time of polymer chain. While for $S\tau_s > 1$, it prefers to be an extended configuration by the action of local flow. Because the direction and amplitude of the local shear in turbulence fluctuates in time randomly and intermittently, the polymers in turbulence manifest the complicated behavior moving along the fluid particle trajectories, indicating the difficulty for understanding their interactions.

In a previous study, we investigated single polymer chain dynamics in isotropic turbulence [22]. We found that the coil-stretch transition occurred for characteristic Weissenberg numbers $W_i = 3 \sim 4$, where the Lagrangian correlation time of the velocity gradient $\nabla \mathbf{u}$ was a key quantity to determine whether the polymers were stretched or not.

We also found that the statistical nature of the polymer chain was well approximated by the dumbbell model. Moreover the relationship between the polymer elongation and local flow topology was discussed by analyzing the statistics of polymer elongation conditioned on the invariants of $\nabla \mathbf{u}$. Although several implications could be drawn from these results, we did not consider the effects of polymer dynamics on turbulence (we considered a one-way coupling regime only). To discuss turbulence modification by polymer additives, we must incorporate the reaction from the enormous number of polymers to the fluid motion.

In the past, turbulent dilute polymer solution flow has mainly been investigated using the constitutive equations like the Oldroyd-B or FENE-P equations [23]. These are the evolution equations for the field of polymer conformation tensor and constructed on the basis of the simple polymer model [23]. The constitutive equations have widely been used for the investigations of turbulence drag reduction [24, 25, 26, 27, 28, 29] or the elastic turbulence [30] because of the easiness to handle the polymers effects on turbulence by the numerical simulations. Recent study pointed out that the resolution condition much more stringent than that of velocity field is required for the adequate computation of FENE-P equation [31].

The hybrid approach, the fluid motion is computed using the Navier-Stokes (NS) equation while the polymers dynamics is done by the molecular dynamics or Brownian dynamics simulations of the appropriate polymer model [23, 32], is the new trend for investigating the dilute polymer solution flow. There were several studies for this issue using the combination of computational fluid dynamics with particle-based simulations of polymer model with/without the reaction to fluid motion [33, 34, 35, 36, 37, 38]. The advantage of hybrid approach is that we can construct the polymer solution model having rich variety of rheological properties by introducing several interacting forces among beads. Moreover it may be suitable to investigate the phenomena that the Lagrangian view is an intrinsic; the diffusion of polymer solution in turbulent boundary layer [39] or the effects of the degradation of polymers on turbulence [40]. While the disadvantage is that the computational cost becomes much larger as the number of polymer is increased. However we can neglect the interaction among polymers in the case for the dilute solution, implying the computational cost for evaluating forces among particles is proportial to the number of polymers. Then we can perform the efficient simulations for the enormous number of polymers in turbulence using the large-scale parallel computations.

The purpose of the present study is to explore two-way coupled simulation methods using the hybrid approach. The Brownian dynamics simulation for the polymer chain model coupled with the direct numerical simulation (DNS) of turbulent flow were performed using large-scale parallel computations. We used the dumbbell model for the long chain polymer because the dumbbell model can satisfactorily reproduce the overall results obtained by the chain model [22, 31]. To gain the significant reaction from polymers to fluid, we needed a much large number of dumbbells in the flow domain. In this study the enormous number ($O(10^9)$) of dumbbells were dispersed in turbulent flow, and their advections and deformations were strictly tracked during the time evolution. Then we examined the degree of modification of turbulent flow by investigating the concentration and Weissenberg number effects on the fundamental quantities and the vortical structures in the case for decaying isotropic turbulence. Because there is no mean shear in isotropic turbulence, it is suitable to investigate the effects of polymers on the bulk of turbulence by analyzing the interaction between polymers and the velocity gradient fluctuations.

Modification of isotropic turbulence by polymer additives have been investigated by the DNS of FENE-P model [27, 28, 29]. Making a comparison between the present results and the previous ones obtained by FENE-P model may be useful to assess the hybrid approach introduced in this study. Moreover we examined the validation for the assumption introduced for evaluating the polymer stress field which is added to the NS equation as the reaction term from dumbbells.

This paper is organized as follows. We briefly describe the model equations and numerical method in Secs. 2 and 3. The effects of the polymer additives on decaying turbulence are examined by varying the parameters like concentration and Weissenberg number in Sec. 4. Section 5 is assigned for examining the nature of coherent structures with and without polymers, where the specific structures in the polymer stress field are discussed. The variation of results when the number of polymers is changed are also discussed in Sec. 6. We summarized the main results obtained in this study in Sec. 7.

2 Polymer solution model

2.1 Governing equations

We used the dumbbell model to represent the polymer dynamics dispersed in the flow domain. In this method, each polymer is represented by two beads connected by a nonlinear spring [23]. The interaction among different dumbbells is neglected because we considered dilute polymer solutions. Moreover, we neglected the inertia of the particles because the inertia of the coiled polymer was very small. Thus, the equations of motion for the end-to-end vector $\mathbf{R}^{(n)}(t) = \mathbf{x}_1^{(n)}(t) - \mathbf{x}_2^{(n)}(t)$ and the center of mass vector $\mathbf{r}_g^{(n)}(t) = (\mathbf{x}_1^{(n)}(t) + \mathbf{x}_2^{(n)}(t))/2$ of the n-th dumbbell are respectively given by

$$\frac{d\mathbf{R}^{(n)}}{dt} = \mathbf{u}_1^{(n)} - \mathbf{u}_2^{(n)} - \frac{1}{2\tau_s} f\left(\frac{|\mathbf{R}^{(n)}|}{L_{max}}\right)\mathbf{R}^{(n)} + \frac{r_{eq}}{\sqrt{2}\tau_s}\left(\mathbf{W}_1^{(n)} - \mathbf{W}_2^{(n)}\right), \tag{1}$$

$$\frac{d\mathbf{r}_g^{(n)}}{dt} = \frac{1}{2}\left(\mathbf{u}_1^{(n)} + \mathbf{u}_2^{(n)}\right) + \frac{r_{eq}}{\sqrt{8}\tau_s}\left(\mathbf{W}_1^{(n)} + \mathbf{W}_2^{(n)}\right), \quad \left(\mathbf{u}_\alpha^{(n)} \equiv \mathbf{u}(\mathbf{x}_\alpha^{(n)}(t), t)\right), \tag{2}$$

where $\mathbf{u}(\mathbf{x}, t)$ denotes the velocity field of the solvent fluid. We adopted the finitely extensible nonlinear elastic (FENE) model [23] given by $f(z) = 1/(1-z^2)$. The dumbbell cannot extend beyond the maximum length L_{max}. The term $\mathbf{W}_{1,2}^{(n)}(t)$ indicates a Brownian random force acting on the particles from the solvent fluid, obeying Gaussian statistics with a white-in-time correlation as $\langle W_{\alpha,i}^{(n)}(t)\rangle = 0$, $\langle W_{\alpha,i}^{(m)}(t) W_{\beta,j}^{(n)}(s)\rangle = \delta_{\alpha\beta}\delta_{ij}\delta_{mn}\delta(t-s)$. Here, δ_{ij} denotes the Kronecker delta and $\delta(t)$ is the delta function. τ_s and r_{eq} are the relaxation time and the equilibrium length of the dumbbell under $\mathbf{u}(\mathbf{x}, t) = \mathbf{0}$.

The turbulent velocity field obeys the incompressible Navier-Stokes equation

$$\nabla \cdot \mathbf{u} = 0, \quad \frac{\partial \mathbf{u}}{\partial t} + \mathbf{u} \cdot \nabla \mathbf{u} = -\nabla p + \nu \nabla^2 \mathbf{u} + \nabla \cdot \mathbf{T}^p, \tag{3}$$

where ν is the kinematic viscosity. $\mathbf{T}^p(\mathbf{x}, t)$ is the polymer stress tensor due to the force acting on the fluid from the dispersed dumbbells. It is defined by

$$T_{ij}^p(\mathbf{x}, t) = \frac{\nu\eta}{\tau_s}\left(\frac{L_{box}^3}{N_t}\right)\sum_{n=1}^{N_t}\left[\frac{R_i^{(n)} R_j^{(n)}}{r_{eq}^2} f\left(\frac{|\mathbf{R}^{(n)}|}{L_{max}}\right) - \delta_{ij}\right]\delta(\mathbf{x} - \mathbf{r}_g^{(n)}). \tag{4}$$

$\eta \equiv (3r_{eq}/4a)^2\Phi_V$ is the zero shear contribution of polymers to the total solution viscosity, a is the radius of the bead, and $\Phi_V \equiv (8\pi N_t/3)(a/L_{box})^3$ represents the volume fraction of the ensemble of dumbbells. Thus η is proportional to the polymer concentration.

2.2 Parameter setting

We evaluated how many polymers were required to realize a significant turbulence modification. According to an experimental study using polyacrylamide ($M_p = 18 \times 10^6$ a.m.u.), the number of polymers per box with volume l_K^3, l_K being the Kolmogorov length, can be estimated by $N_K = 3.6 \times 10^6$ when $R_\lambda \simeq 50$ with a 5 ppm solution [10]. Therefore, the total number of polymers in the computational box was estimated as $N_t = N_k(L_{box}/l_K)^3 = O(10^{13})$ when using adequate DNS conditions ($\Delta x = l_K$) for small-scale statistics. The order $N_t = O(10^{13})$ is much too large, even for using a state-of-the-art supercomputer. Thus an approximate method was required to represent the interaction between the fluid and polymers. We supposed that N_t was represented by $N_t = b\tilde{N}_t$, where $\tilde{N}_t$ indicates the total number of dumbbells in the computation and b is an artificial parameter representing the number of "replica dumbbells" per a dumbbell. In this case, the polymer stress tensor was approximated by replacing N_t in (4) by $\tilde{N}_t$.

Dumbbell parameters r_{eq}, a, and L_{max} were determined using experimental parameters [10] under fixed l_K. It is shown in [10] that $R_g = 0.5\mu m$, $L_{max} = 77\mu m$ for polymer solution using Polyacrylamide. Then we evaluated as $L_{max}/l_K = 0.3$, $r_{eq}/l_K = 3.0 \times 10^{-3}$ and $a/l_K = (3\Phi_V/4\pi N_K)^{1/3} = 7.0 \times 10^{-5}$, where we use the relationship $\sqrt{3}r_{eq} \simeq \sqrt{6}R_g$ for Gaussian coil and $l_K \simeq 280\mu m$ when $R_\lambda = 50$. The Weissenberg number W_i controls the elastic nature of the polymer model. It is defined by $W_i = \tau_s/\tau_K$, where τ_K is the Kolmogorov time. In this study W_i is used for the control parameter to determine the elastic nature of dumbbell, i.e. τ_s is determined by using the values of W_i and τ_K.

3 Numerical simulations

Direct numerical simulations (DNSs) of Eqs. (3) were performed in a periodic box with periodicity 2π using the pseudo-spectral method in space and the 2nd order Runge-Kutta method in time. The initial conditions of the velocity field were set to random, obeying Gaussian statistics with an energy spectrum

$$E(k,0) = 16\sqrt{2/\pi}(u_0^2/k_0)\,(k/k_0)^4 \exp\left(-2\,(k/k_0)^2\right) \quad (u_0 = 1, k_0 = 2). \tag{5}$$

The total number of grid points for DNS were set to $N^3 = 128^3$. The Taylor micro-scale Reynolds number $R_\lambda(t)$ was $R_\lambda(0) = 52$, which monotonically decayed with time. In this process, the decaying turbulence was approximately regarded as statistically isotropic and homogeneous. $l_K(t) = (\nu^3/\epsilon(t))^{1/4}$, where $\epsilon(t)$ is the energy dissipation rate, was always larger than the grid spacing Δx, *i.e.*, the velocity field was adequately smooth at small scales. $\tau_K = (\nu/\epsilon(t))^{1/2}$ and l_K used for determining several parameters are evaluated using the maximum value ϵ_{max} of $\epsilon(t)$ in the one-way coupling case.

Initial positions of dumbbells were uniformly distributed over the computational domain by using uniform random numbers. The initial configuration of each dumbbells were

Table 1: Parameters for DNS of decaying turbulence and Brownian dynamics simulation for dispersed dumbbells. Run 0 means the one-way case.

	$\tilde{N}_t$ ($\times 10^9$)	b ($\times 10^5$)	Φ_V($\times 10^{-4}$)	η	W_i
Run 0	1.008	0	0	0	5
Run E1	0.504	0.9	1.01	0.1045	5
Run E2	1.008	0.9	2.02	0.2090	5
Run W1	0.504	0.9	1.01	0.1045	1
Run W2	0.504	0.9	1.01	0.1045	15
Run L	0.126	7.2	2.02	0.2090	5
Run H	8.064	0.1125	2.02	0.2090	5

set by $\mathbf{R}^{(m)}(0) = r_{eq}\mathbf{n}^{(m)}$ where $\mathbf{n}^{(m)}$ was the unit random vector taken over the all orientations. Time integration of eqs. (1) and (2) were performed by using the similar scheme proposed in [11], where the velocity components at each bead position were interpolated using a TS13 scheme [41]. Multi-scale method was used for the temporal evolution of $\mathbf{R}^{(n)}(t)$, where the time increment Δt_p for $\mathbf{R}^{(n)}(t)$ was chosen by $\Delta t_p = \Delta t_{DNS}/5$ when $|\mathbf{R}^{(n)}(t)| > 0.9L_{max}$, while $\Delta t_p = \Delta t_{DNS}$ for $|\mathbf{R}^{(n)}(t)| < 0.9L_{max}$.

Parallel computations were used to evaluate the convection and deformation of the dispersed dumbbells. The total number of dumbbells $\tilde{N}_t$ was divided into m groups, and their temporal evolution was individually computed for each node. One node was assigned to the DNS of the solvent fluid, so that we used $m+1$ processes for the parallel computation of the fluid-particle system. $\mathbf{u}(\mathbf{x}, t)$ computed in the fluid node was transferred to the other nodes for the polymer computations. The program code was parallelized by using MPI, where the 256 processer elements were used for the parallel computations. The reaction from the polymers was evaluated as follows. 1) The polymer stress field $\mathbf{T}^p_{node}(\mathbf{x})$ was computed according to Eq. (4) in each process. 2) These were gathered to the process for fluid computation and summed. 3) The obtained $\mathbf{T}^p(\mathbf{x})$ was incorporated into the DNS scheme. In the step 1), because the center of mass vector $\mathbf{r}_g^{(n)}$ for each dumbbells were not on the grid points for DNS computation, we needed some approximate expression instead of Eq. (4). The delta function in Eq. (4) was approximated by the weight function which was the function of surrounded 8 grid points around $\mathbf{r}_g^{(n)}$ and determined by the weights used for linear interpolation scheme [42].

Elastic nature of dumbbells is controlled by changing W_i, and the concentration of polymer solution is determined by the value of η. In this study we performed the series of simulations as 1) η dependence under fixed W_i, 2) W_i dependence under fixed η, and 3) $\tilde{N}_t$ dependence under fixed W_i, η and N_t. The parameters used for simurations are summarized in Table 1.

4 Modification of decaying isotropic turbulence

4.1 Concentration effect

We examined the modification of the turbulent polymer solution flow by changing η under fixed W_i (= 5). Figure 1 shows the temporal evolution of the kinetic energy $E(t) = \langle u_i^2 \rangle/2$

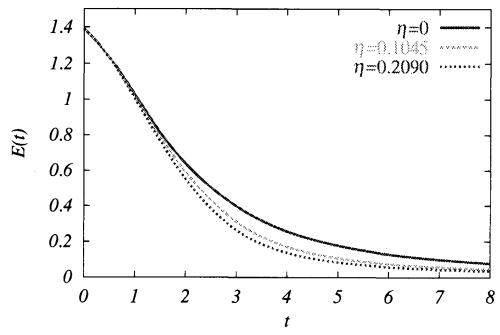

Figure 1: η effect on the temporal evolution of the kinetic energy $E(t)$.

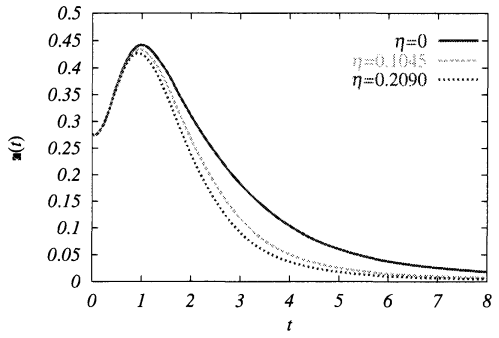

Figure 2: η effect on the temporal evolution of the energy dissipation rate $\epsilon(t)$.

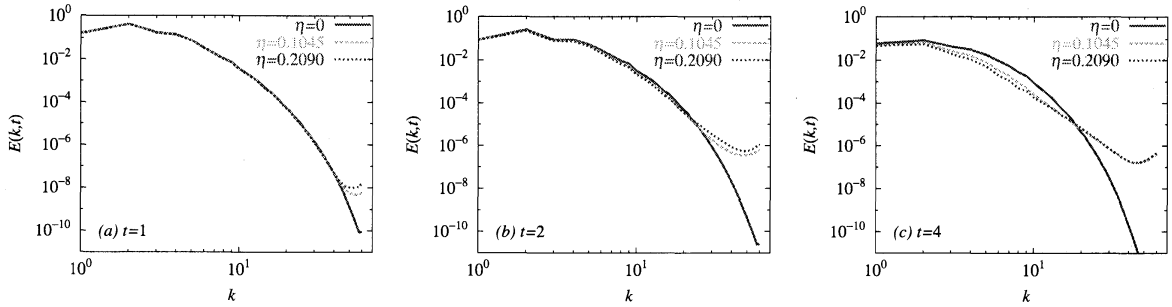

Figure 3: Comparison of the behavior of the kinetic energy spectrum $E(k,t)$ obtained by Runs 0, E1 and E2; (a) $t = 1$, (b) $t = 2$ and (c) $t = 4$.

in the cases for $\eta = 0$ (Run 0), 0.1045 (Run E1) and 0.2090 (Run E2). Kinetic energy monotonically decayed with time, and the decay rate increased with increase of η. Figure 2 indicates the temporal evolutions for the energy dissipation rate $\epsilon(t)$. Peak positions located around $t = 1$ irrespective of η, and $\epsilon(t)$ decayed with time for $t > 1$, where the reduction rate of $\epsilon(t)$ became larger as η increased. These observations suggest that the extension of dumbbells affected to the scales of turbulent motions over the entire wavenumber range, being qualitatively consistent with the DNS results using a FENE-P model [27].

To see these modifications in more details, we investigated the behavior of the kinetic energy spectrum $E(k,t)$. Figure 3 indicates the comparison of $E(k,t)$ for Runs 0–2 in the cases for (a) $t = 1$, (b) $t = 2$ and (c) $t = 4$. The spectral behavior was deformed by the polymer additives within its tail part up to $t = 1$, and the deviation from the one-way result became larger with increase of η. At the final period of decay, the spectral modification was observed over the entire wavenumber range, suggesting the energy transfer dynamics was affected even in the larger scales by the modification of dissipation mechanism in the smaller ones.

As shown in the aforementioned results, turbulence modification was originated from the reaction due to the dumbbell dynamics which was characterized by the statistical nature of the ensemble of dumbbells. Next we investigate the temporal evolutions of the probability density function (PDF) for the dumbbell end-to-end distance $|\mathbf{R}^{(n)}|$. These were plotted in Fig. 4 for Runs 0–2 in the cases for (a) $t = 1$, (b) $t = 2$ and (c) $t = 4$,

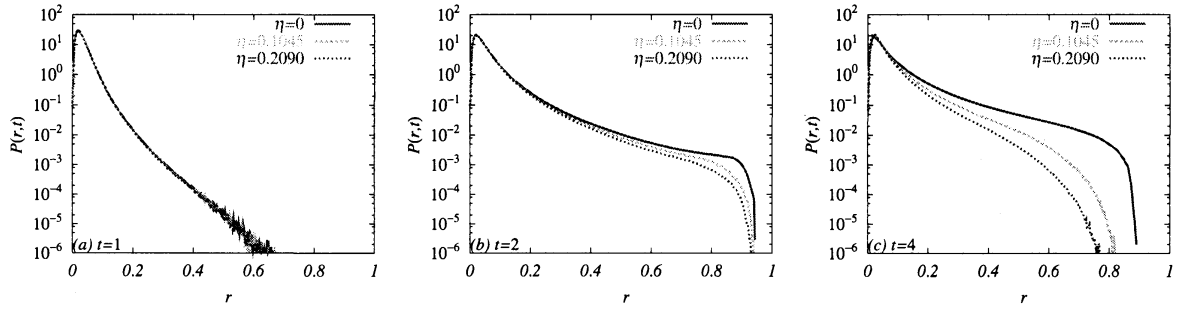

Figure 4: η effect on the temporal evolution of the polymer extension PDF $P(r,t)$; (a) $t = 1$, (b) $t = 2$ and (c) $t = 4$.

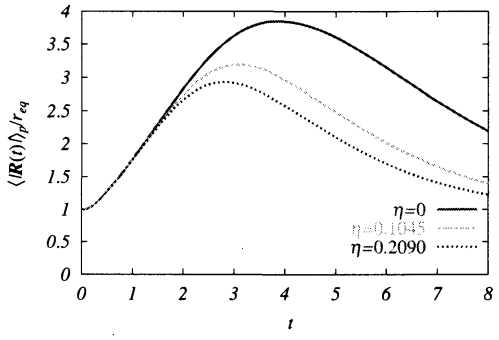

Figure 5: Variation of the temporal evolution of mean extension $\langle|\mathbf{R}|\rangle_p/r_{eq}$ against η.

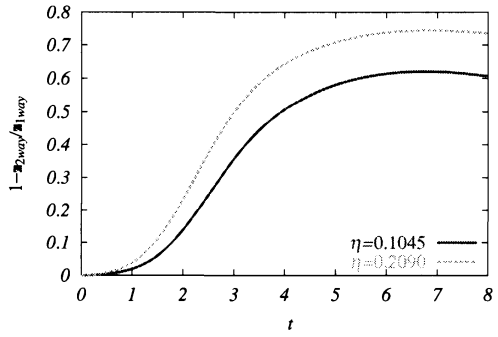

Figure 6: Variation of the temporal evolution of reduction rate of $\epsilon(t)$ against η.

where $|\mathbf{R}^{(n)}|$ was normalized by L_{max}. The curves in (a) were almost the same irrespective of η and the peak position located near zero, indicating the reaction to turbulence was almost negligible when $t \leq 1$. We could observe a lot of stretched dumbbells as the time goes on, where they were more stretched as decreasing η. The reduction of the number of stretched dumbbells with increase of η is explained by the fact that the velocity gradient fluctuation is more suppressed as η increases, as shown in Fig. 2. Figure 5 indicates the time evolutions of the mean dumbbell extension normalized by r_{eq}. The curve obtained by Run 0 represented that the passively advected dumbbells were more stretched than two-way cases. This observation was almost consistent with the results by DNS of constitutive equations [24, 27]. It is interesting to notice that the time $|\mathbf{R}^{(n)}|$ approaches to their maximum values is later than those for the energy dissipation rate $\epsilon(t)$ (Fig. 2).

We examined the percentage reduction rate of $\epsilon(t)$. This is defined by $1 - \epsilon_{2way}/\epsilon_{1way}$. The resulting curves are shown in Fig. 6. More reductions were observed in the final period of decay, irrespective of η. The reduction rate increased with increase of η, suggesting the intensity of reaction by dumbbells became bigger as η increased.

4.2 Weissenberg number effect

In this subsection, we examined the degree of turbulence modification by changing Weissenberg number W_i under fixed η (= 0.1045). Figure 7 shows the temporal evolutions of $E(t)$ for the cases with $W_i = 1$ (Run W1),5 (Run E1) and 15 (Run W2). The curves

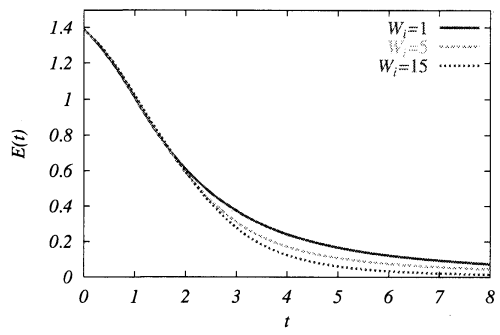

Figure 7: W_i effect on the temporal evolution of the kinetic energy $E(t)$.

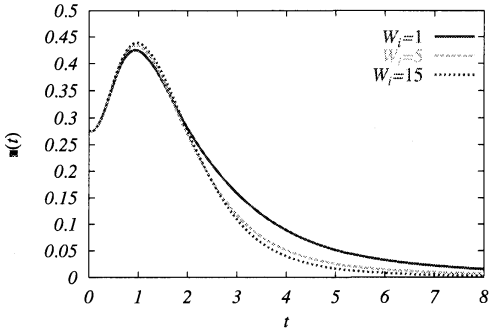

Figure 8: W_i effect on the temporal evolution of the energy dissipation rate $\epsilon(t)$.

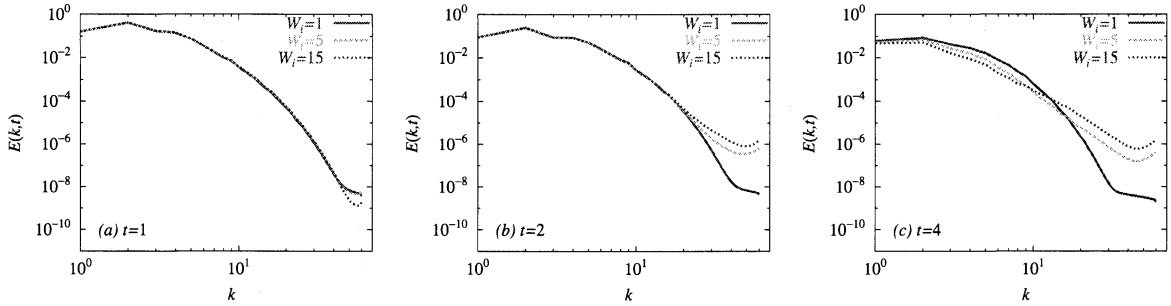

Figure 9: Comparison of the behavior of the kinetic energy spectrum $E(k,t)$ obtained by Runs W1, E1 and W2; (a) $t = 1$, (b) $t = 2$ and (c) $t = 4$.

almost collapsed on the same when $t < 2$. While for $t > 2$, the larger W_i cases decayed faster than the smaller ones. Comparison of the temporal evolutions of the energy dissipation rate $\epsilon(t)$ is shown in Fig. 8. More energy dissipation reduction in the case for the larger W_i could be clearly seen for $t > 2$. These facts suggest that the dumbbells were more stretched for larger W_i, leading to the more significant reactions.

Weissenberg number effect on the spectral modification were examined by comparing the behavior of kinetic energy spectrum $E(k,t)$ for various W_i. Figure 9 shows the resulting curves for the cases (a) $t = 1$, (b) $t = 2$ and (c) $t = 4$. As the time increased, the collapsing region was shrinking in the high wavenumber range. It should be noted that W_i-dependence at $t = 4$ was very similar to the DNS results of FENE-P model with isotropic steady turbulence [28]. The spectral behavior at $t = 4$ for $W_i = 1$ was entirely different from that for $W_i = 15$ which had the near power law decay in the whole wavenumber range. Because the turbulence adequately decayed while the mean elongation of dumbbells had the maximum value around $t = 4$, we think the spectral dynamics is dominated by the elastic nature of the ensemble of dumbbells rather than the nonlinear term of NS equation. We may need more detailed analysis to draw the definite statement by investigating the transfer properties in the wavenumber space.

Comparison of the PDF behavior for the dumbbell elongation are shown in Fig. 10 for (a) $t = 1$, (b) $t = 2$ and (c) $t = 4$. Extension of dumbbells became larger as W_i increased. For $W_i = 15$, it was seen that there were a lot of dumbbells having more stretched configurations. In the decay regime of $\epsilon(t)$ ($t > 2$), the fully stretched dumbbells

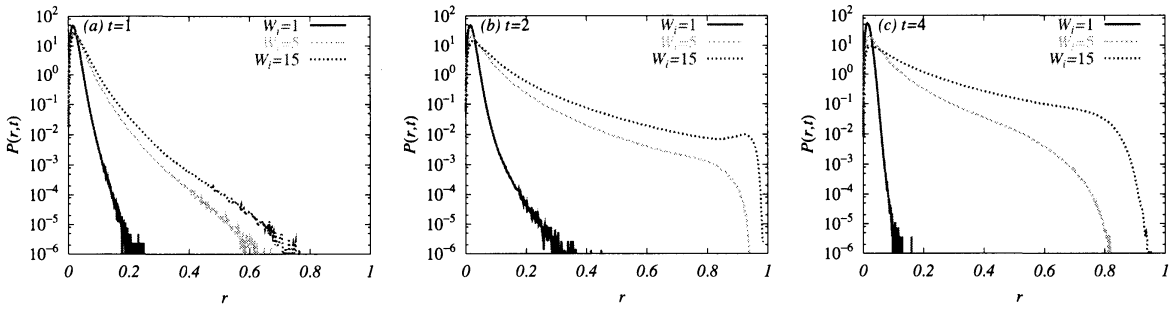

Figure 10: W_i effect on the temporal evolution of the polymer extension PDF $P(r,t)$; (a) $t = 1$, (b) $t = 2$ and (c) $t = 4$.

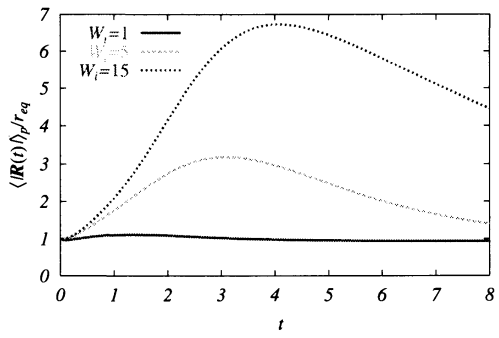

Figure 11: Variation of the temporal evolution of mean extension $\langle |\mathbf{R}| \rangle_p / r_{eq}$ against W_i.

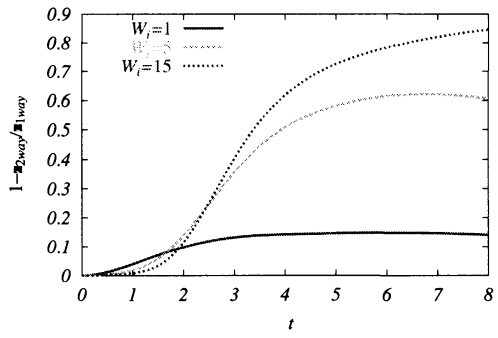

Figure 12: Variation of the temporal evolution of reduction rate of $\epsilon(t)$ against W_i.

shrunk toward equilibrium state. This was clearly seen in Fig. 11 where the temporal evolutions of the mean end-to-end distance of dumbbell normalized by r_{eq} were plotted. The mean extension for $W_i = 1$ was near r_{eq} in the whole time region, while for $W_i = 15$ it sharply increased until $t = 4$ and gradually decayed for $t > 4$. Because the larger extensions of dumbbells can lead to the larger effects on turbulence, it was plausible that the more energy dissipation reduction was observed for larger W_i. The percentage of energy dissipation reduction rate was plotted in Fig. 12 as the function of t for various W_i. The reduction rate became larger as W_i was increased for $t > 2$. Thus we concluded that the larger W_i solution flow was more efficient reducer of the intensity of turbulent velocity gradient fluctuations, being consistent with the results in [28].

5 Comparison of coherent structures

The intuitive way to examine the impact of polymer additives on turbulence is to see the modification of coherent structures appeared in the turbulent field. In this section we investigate the η and W_i effects on the vortical structures. Moreover the specific character of field structure in the polymer stress tensor is discussed.

Figure 13 shows the comparison of vortical structures obtained by Run 0 and Run E1 at $t = 3.5$, where they were visualized by using the second invariant Q of the velocity gradient tensor $\nabla \mathbf{u}$. Figure indicated that although the whole view of structures were

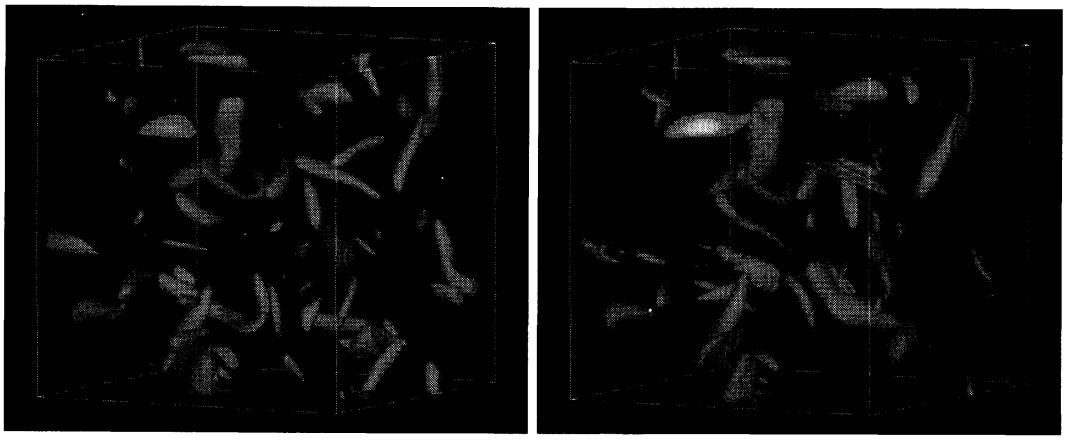

Figure 13: Comparison of the iso-surface of Q for $\eta = 0$ (left: Run 0) and $\eta = 0.1045$ (right: Run E1) at $t = 3.5$. Iso-surface level is chosen by $Q/Q_{rms} = 3$.

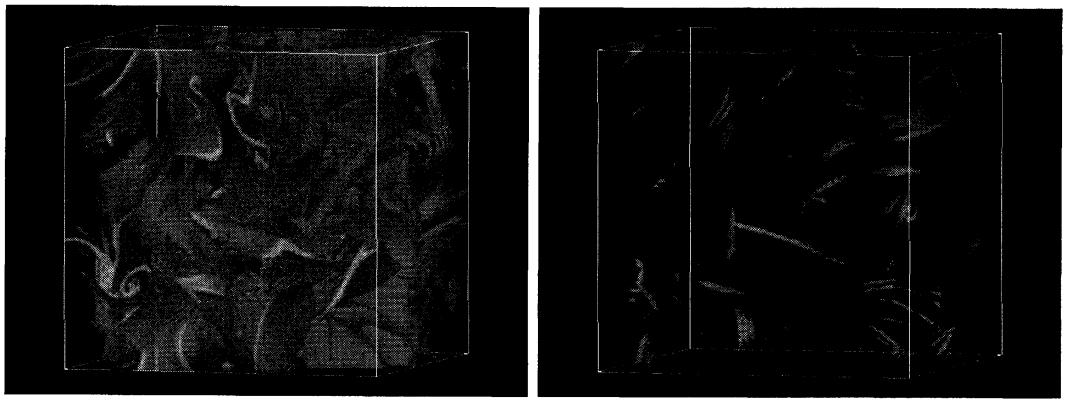

Figure 14: Iso-surface of the trace of polymer stress tensor $X = T_{ii}^p$ obtained by Run E2 at $t = 3.5$. Iso-surface level is chosen by $X/X_{rms} = 1.5$ (left) and $X/X_{rms} = 6$ (right).

indistinguishable each other, the generation of intense structures for Run E1 was suppressed more than the case for Run 0. This fact was consistent with the observation for the reduction of energy dissipation in Fig. 2. Also the similar results were obtained in the DNS studies of FENE-P equation [27, 29]

Figure 14 illustrates the iso-surface of the trace of the polymer stress tensor T_{ii}^p obtained by Run E2 at $t = 3.5$. It was recognized that the region for the intermediate intensity of T_{ii}^p had the peculiar sheet-like structures which nearly located among intense regions of $Q(> 0)$. While for the region of larger value of T_{ii}^p the filament-like structures were observed. Thus the characteristic structure of T_{ii}^p is dependent on the intensity of fluctuation. Sheet-like structures could be clearly seen in Fig. 15 where the two dimensional slice of Fig. 14 were visualized. This observation reminds us the sheet-like structures observed in the scalar gradient field of the passive scalar turbulence. In fact, the amplification mechanism of scalar gradient vector is similar for that of the end-to-end vector of dumbbell. We need further analysis to clarify this observation by investigating the relationship between the velocity gradient and the end-to-end vector of dumbbell.

Figure 15: Comparison of the 2D slice between Q (left) and T_{ii}^p (right) obtained by Run E2 at $t = 3.5$.

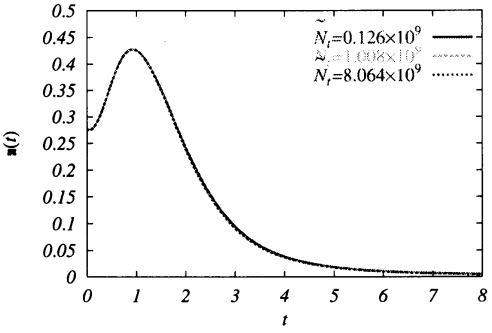

Figure 16: Comparison of the time evolution of $\epsilon(t)$ for Runs L, E2 and H.

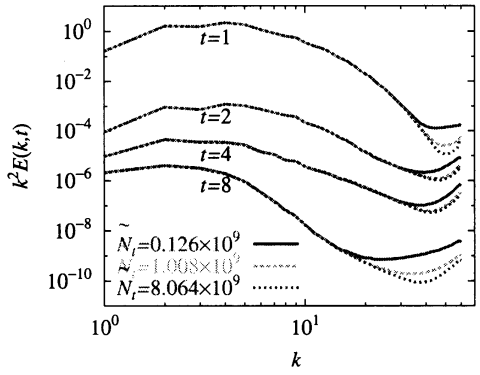

Figure 17: Behavior of the dissipation spectra $k^2E(k,t)$ obtained by Runs L, E2 and H.

6 Validation of assumption for polymer stress field

We assumed that there were many "replica" dumbbells to construct the polymer stress field from dumbbell configurations because we need much larger computational resources to realize the reactions from the enormous number of dumbbells dispersed in the flow domain. It is indispensable to know how many dumbbells are needed to realize the adequate results in the statistical sense. For this issue, in this section, we examined the effects of the variation of b and $\tilde{N}_t$ under fixed N_t.

The comparison of the curves for temporal evolutions of $\epsilon(t)$ for Runs L, E2 and H is shown in Fig. 16. It was seen that they were almost the same. Curves for the dissipation spectra $k^2E(k,t)$ are also shown in Fig. 17. The spectral behavior was indistinguishable except for the spectral tails. The deviation in the high wavenumber range may be attributed to an insufficient number of dumbbells to obtain smooth variations of $\mathbf{T}^p$ on the grid scale. Figure 18 compares coherent vortices visualized using the iso-surface of the second invariant Q of the velocity gradient tensor. Remarkable zig-zag structures were observed in the vortices for Run L compared to Run H, although the entire trends of the structures were quite similar.

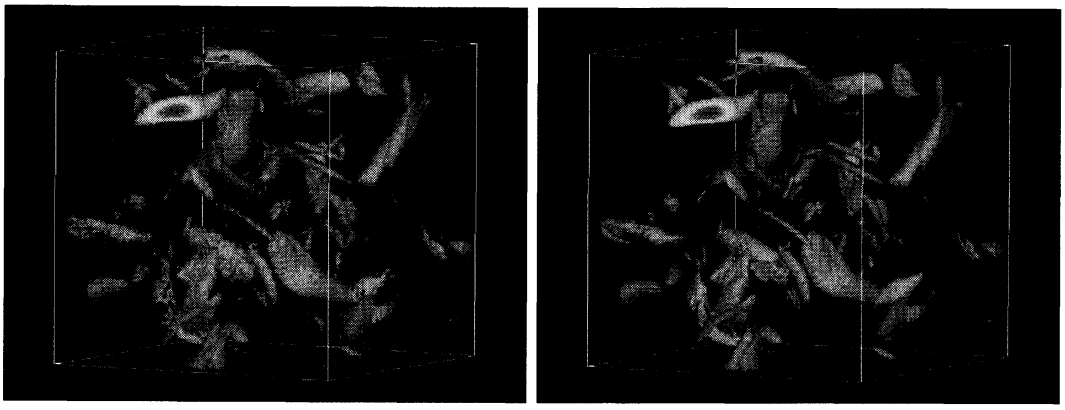

Figure 18: Comparison of iso-surface visualizations of vortical structures using Q with the level $Q/Q_{rms} = 2.5$ (left: Run L, right: Run H) at $t = 3.5$.

These results suggest that the "replica assumption" introduced for the evaluation of $\mathbf{T}^p$ works very well as far as the large-scale nature of turbulence is concerned. However, many more dumbbells are required for better prediction of the turbulence modification around the Kolmogorov scale.

7 Conclusions

The parallel computations for turbulent polymer solution flow were performed by using the hybrid approach; Brownian dynamics simulation of polymer model (dumbbells) coupled with the DNS of the NS equation. We examined the turbulence modification by the enormous number of dumbbells ($O(10^9)$) dispersed in decaying isotropic turbulence. As a result, we observed a significant energy dissipation reduction and energy spectrum modification in the later stages of decay when the concentration of polymers or the Weissenberg number was increased. These were entirely consistent with the results of DNS using a constitutive equation [27, 29].

Visualization of coherent vortices using the second invariant Q of $\nabla \mathbf{u}$ clarified that the generation of intense vortices were suppressed by polymer additives. This was consistent with the observation for the reduction of energy dissipation rate. We also showed that the region having longer dumbbell extension had the sheet-like or filament-like structures located among intense vortices. This implies that the stretching polymers almost locate in the $Q < 0$ region which was dominated by the strain. This was consistent with the results of our previous study in which the conditional mean distance of polymer chain on Q and R had a large value in the region $Q < 0, R > 0$ [22].

We found that the spectral tails were most affected by polymer additives in which the degree of modification was dependent on the parameters b and $\tilde{N}_t$, even though $N_t = b\tilde{N}_t$ was fixed. This nature was clearly confirmed by the visualization of vortical structures, where the smaller $\tilde{N}_t$ results had a rough surface on the vortices due to the insufficient evaluation of $\mathbf{T}^p$ on grid scales.

The results obtained in this study represent that the hybrid approach with the parallel computation is very effective for investigating the dilute polymer solution flows. Although

we used the dumbbell model for the long chain polymer, it is interesting to introduce more realistic polymer chain model having the hydrodynamic interaction or excluded volume forces among beads [32]. Hybrid approach has a great advantage for examining the effect of these extra forces on turbulence modification whose issue cannot be touched by the constitutive equation. This would be the subject of future work.

T.W. and T.G's work was partially supported by Grants-in-Aid for Scientific Research Nos. 20760112 and 21360082, respectively, from the Ministry of Education, Culture, Sports, Science, and Technology of Japan. T.W. thanks S. Uno and D. Sugimoto for their assistances of making parallelized code. The authors thank the Theory and Computer Simulation Center of the National Institute for Fusion Science and the Information Technology Center of Nagoya University for their computational support.

References

[1] J. L. Lumley, J. Polymer Sci.: Macromolecular Reviews **7**, 263–290 (1973).

[2] K. R. Sreenivasan and C. M. White, J. Fluid Mech. **409**, 149–164 (2000).

[3] I. Proccacia, V. S. L'vov and R. Benzi, Rev. Mod. Phys. **80**, 225–247 (2008).

[4] A. Groisman and V. Steinberg, Nature **410**, 905–908, (2001)

[5] T. Burghelea, E. Segre, and V. Steinberg, Phys. Rev. Lett. **92**, 164501 (2004).

[6] P. E. Arratia, C. C. Thomas, J. Diorio, and J. P. Gollub, Phys. Rev. Lett. **96**, 144502 (2006).

[7] A. Groisman and V. Steinberg, Nature **405**, 53–55, (2000)

[8] T. Burghelea, E. Segre, and V. Steinberg, Phys. Rev. Lett. **96**, 214502 (2006).

[9] Y. Jun and V. Steinberg, Phys. Rev. Lett. **102**, 124503 (2009).

[10] N. T. Ouellette, H. Xu and E. Bodenschatz, J. Fluid Mech. **629**, 375–385 (2009).

[11] A. Celani, A. Puliafito, and K. Turitsyn, Europhys. Lett. **70**, 464–470 (2005).

[12] M. Chertkov, I. Kolokolov, V. Lebedev, and K. Turitsyn, J. Fluid Mech. **531**, 251–260 (2005).

[13] S. Gerashchenko and V. Steinberg, Phys. Rev. Lett. **96**, 038304 (2006).

[14] M. Chertkov, Phys. Rev. Lett. **84**, 4761–4764 (2000).

[15] E. Balkovsky, A. Fouxon, and V. Lebedev, Phys. Rev. Lett. **84**, 4765–4768 (2000).

[16] J-L. Thiffeault, Phys. Lett. A **308**, 445-450 (2003).

[17] M. M. Afonso and D. Vincenzi, J. Fluid Mech. **540**, 99–108 (2005).

[18] A. Celani, S. Musacchio and D. Vincenzi, J Statis. Phys. **118**, 531–554 (2005).

[19] S. Gerashchenko, C. Chevallard, and V. Steinberg, Europhys. Lett. **71**, 221–227 (2005).

[20] Y. Liu and V. Steinberg, Europhys. Lett. **90**, 44005 (2010).

[21] P. G. De Gennes, J. Chem. Phys. **60**, 5030–5042 (1974).

[22] T. Watanabe and T. Gotoh, Phys. Rev. E **81**, 066301 (2010).

[23] R. B. Bird, C. F. Curtiss, R. C. Amstrong, and O. Hassager, *Dynamics of Polymetric Liquids, Vol.2 Kinetic Theory*, 2nd ed. (Wiley, New York, 1987).

[24] B. Eckhardt, J. Kronjager, and J. Schumacher, Comput. Phys. Commun. **147**, 538–543 (2002).

[25] J. J. J. Gillissen, Phys. Rev. E **78**, 046311 (2008).

[26] S. Tamano, M. Itoh, S. Hotta, K. Yokota, and Y. Morinishi, Phys. Fluids **21**, 055101 (2009).

[27] P. Perlekar and D. Mitra and R. Pandit, Phys. Rev. Lett. **97**, 264501 (2006).

[28] P. Perlekar and D. Mitra and R. Pandit, Phys. Rev. E **82**, 066313 (2010).

[29] W.-H. Cai, D.-C. Li and H.-N. Zhang, J. Fluid Mech. **665**, 334–356 (2010).

[30] G. Boffetta, A. Celani, and S. Musacchio, Phys. Rev. Lett. **91**, 034501 (2003).

[31] S. Jin and L. R. Collins, New J. Phys. **9**, 360 (2007).

[32] M. Doi and S. F. Edwards, *The Theory of Polymer Dynamics*, (Oxford University Press, New York, 1986).

[33] M. Laso and H. C. Ottinger, J. Non-Newtonian Fluid Mech. **47**, 1–20 (1993).

[34] P. A. Stone and D. Graham, Phys. Fluids **15**, 1247–1256 (2003).

[35] V. E. Terrapon, Y. Dubief, P. Moin, E. S. G. Shaqfeh, and S. K. Lele, J. Fluid Mech. **504**, 61–71 (2004).

[36] J. Davoudi and J. Schumacher, Phys. Fluids **18**, 025103 (2006).

[37] T. Peters and J. Schumacher, Phys. Fluids **19**, 065109 (2007).

[38] S. Yasuda and R. Yamamoto, Phys. Rev. E **81**, 036308 (2010).

[39] B. R. Elbing, D. R. Dowling, M. Perlin, and S. L. Ceccio, Phys. Fluids **22**, 045102 (2010).

[40] H. J. Choi, S. T. Lim, Pik-Yin Lai and C. K. Chan Phys. Rev. Lett. **89**, 088302 (2002).

[41] P. K. Yeung and S. B. Pope, J. Comp. Phys. **79**, 373–416 (1988).

[42] A. Prosperetti and G. Tryggvason (Eds.), *Computational Methods for Multiphase Flow*, (Cambridge University Press, Cambridge, 2007).